

# Elliptical-tube off-beam quartz-enhanced photoacoustic spectroscopy

Cite as: Appl. Phys. Lett. **120**, 171101 (2022); <https://doi.org/10.1063/5.0086697>

Submitted: 28 January 2022 • Accepted: 09 April 2022 • Published Online: 25 April 2022

Zhijin Shang, Hongpeng Wu, Shangzhi Li, et al.



View Online



Export Citation



CrossMark

## ARTICLES YOU MAY BE INTERESTED IN

[Color-tunable organic light-emitting diodes with ultrathin thermal activation delayed fluorescence emitting layer](#)

Applied Physics Letters **120**, 171102 (2022); <https://doi.org/10.1063/5.0084137>

[Realizing single-mode lasing in all-inorganic CsPbBr<sub>3</sub> perovskite microwires using intrinsic self-absorption](#)

Applied Physics Letters **120**, 171105 (2022); <https://doi.org/10.1063/5.0085422>

[A 5.7 THz GaN/AlGaN quantum cascade detector based on polar step quantum wells](#)

Applied Physics Letters **120**, 171103 (2022); <https://doi.org/10.1063/5.0086641>

Timing is everything.  
Now it's automatic.

A new synchronous source measure system for electrical measurements of materials and devices

**Lake Shore**  
CRYOTRONICS

[Learn more](#)

# Elliptical-tube off-beam quartz-enhanced photoacoustic spectroscopy

Cite as: Appl. Phys. Lett. **120**, 171101 (2022); doi: [10.1063/5.0086697](https://doi.org/10.1063/5.0086697)

Submitted: 28 January 2022 · Accepted: 9 April 2022 ·

Published Online: 25 April 2022




View Online



Export Citation



CrossMark

Zhijin Shang,<sup>1,2</sup> Hongpeng Wu,<sup>1,2</sup> Shangzhi Li,<sup>1,2</sup> Frank K. Tittel,<sup>3</sup> and Lei Dong<sup>1,2,a)</sup> 

## AFFILIATIONS

<sup>1</sup>State Key Laboratory of Quantum Optics and Quantum Optics Devices, Institute of Laser Spectroscopy, Shanxi University, Taiyuan 030006, China

<sup>2</sup>Collaborative Innovation Center of Extreme Optics, Shanxi University, Taiyuan 030006, China

<sup>3</sup>Department of Electrical and Computer Engineering, Rice University, 6100 Main Street, Houston, Texas 77005, USA

<sup>a)</sup> Author to whom correspondence should be addressed: [donglei@sxu.edu.cn](mailto:donglei@sxu.edu.cn)

## ABSTRACT

We propose an elliptical-tube off-beam quartz-enhanced photoacoustic spectroscopy (EO-QEPAS) method in which an elliptical tube is employed as an acoustic resonator, instead of a circular resonator in QEPAS, to match the stripe-like beam emitted from a high-power multi-mode laser diode (MLD). A lower noise level than that of conventional QEPAS is achieved due to the optimal matching between the elliptical resonator and the beam profile, hence resulting in a  $\sim 3$  times higher signal-to-noise ratio gain factor compared with the circular resonator. The parameters of the elliptical resonator are optimized, and a  $1\sigma$  normalized noise equivalent absorption coefficient of  $3.4 \times 10^{-8} \text{ cm}^{-1} \text{ W/Hz}^{1/2}$  is obtained for dry  $\text{NO}_2$  detection at normal atmospheric pressure. EO-QEPAS paves the way for developing compact, cost-effective, and highly sensitive gas sensors based on the combination of MLDs and QEPAS.

Published under an exclusive license by AIP Publishing. <https://doi.org/10.1063/5.0086697>

Trace gas sensing based on photoacoustic spectroscopy (PAS) is widely used in many fields, such as atmospheric environment monitoring, industrial process control, and medical diagnosis due to its high sensitivity and compact structure.<sup>1–6</sup> Quartz-enhanced photoacoustic spectroscopy (QEPAS), which was first proposed in 2002, retains the inherent zero-background and laser wavelength independence of PAS.<sup>7–17</sup> The key innovation of QEPAS is the use of a small-sized, high-Q-factor quartz tuning fork (QTF) as a piezoelectric acoustic transducer offering a high immunity to environmental noise.

Multimode laser diodes (MLDs) are small-sized, inexpensive, and high-power laser sources, which are available from both single emitters and diode arrays at power output levels ranging from tens of milliwatts to hundreds of watts and come in either free space or fiber coupled configurations. Combination of MLDs and QEPAS has the potential to realize a compact, cost-effective, and highly sensitive gas sensor, since the detection sensitivity of QEPAS is proportional to its optical excitation power. However, a QEPAS system has strict requirements on its laser beam quality due to the gap limit of  $\sim 0.3$  mm between commercial QTF prongs, which cannot be usually met by MLDs characterized by large divergence angles and stripe-like emission spots. When the stray light from a MLD irradiates an acoustic transducer, intense noise interference can be introduced.

Electrical/optical modulation cancellation methods (E/O-MOCAMs) and custom QTFs with large prong spacing had been proposed to address the issue of the noise interference.<sup>18–23</sup> Nevertheless, E/O-MOCAMs require an additional electrical/optical noise cancellation system, which results in a degraded long-term stability<sup>18</sup> as well as a large and complex system.<sup>19</sup> These custom QTFs with large geometric dimensions normally have a low resonant frequency, which must be paired with a long acoustic resonator. As a result, the design of the custom QTFs with large prong gap does not allow reaching the miniaturization characteristics of the traditional QEPAS sensor.

An alternative approach to reducing the background noise is to use the off-beam configuration of acoustic resonators in which a thin stainless-steel tube with a slit in the middle as the acoustic resonator is placed on the side of a QTF.<sup>24</sup> A laser beam passes through the inside of the acoustic resonator, instead of passing through the QTF prong gap in the on-beam configuration, thus removing the restriction of the QTF prong gap. The generated sound wave diffuses into the QTF's prongs through the slit of the acoustic resonator and then excites the QTF and generates the photoacoustic signal. In this off-beam configurations, the optical alignment becomes simple and the noise interference is effectively suppressed. However, the laser beams emitted from MLDs are stripe-like beams, which have a mismatch problem with the

circular resonator,<sup>25–27</sup> resulting in unwanted background noise. In fact, acoustic modes of sound waves can be excited in an elliptical tube,<sup>6</sup> which can be used as an appropriate resonator for MLDs, instead of a conventional circular resonator.

In this Letter, we reported elliptical-tube off-beam QEPAS (EO-QEPAS), which is proposed for MLDs as excitation laser sources in QEPAS. An elliptical resonator is designed to work together with the stripe-like beam emitted from a MLD and is assembled with a QTF in the off-beam configurations as an acoustic detection module (ADM). The optimal matching between the elliptical resonator and the beam profile ultimately results in higher signal-to-noise ratio (SNR) gain factor than achievable with the traditional QEPAS system based on the circular resonator.

In order to demonstrate this technique, a commercial high-power long-stripe 450 nm MLD (ORSAM, Model PLTB450) was used to detect NO<sub>2</sub>. The MLD has beam divergence of  $\theta_{\perp} \sim 25^{\circ}$ ,  $\theta_{\parallel} \sim 15^{\circ}$ . A quartz lens with a focal length of 60 mm was utilized to converge the laser beam. An image of the laser spot shape captured at a distance of  $\sim 15$  cm from the lens as shown in Fig. 1(a). The laser spot size at a different distance from the lens was measured by a beam profiling camera (Ophir, Model Pyrocam IIIHR), and the obtained results are shown in Fig. 1(b). All measurements were operated along the axis of the beam propagation, and the center of the MLD emitter was defined as the zero point of the x-axis and y-axis. The minimum length and width of the laser spot were located at the focal point of the lens, which were 490 and 270  $\mu\text{m}$ , respectively.

The structure of an ADM is shown in Fig. 2. A standard 32.7-kHz QTF is placed on the outside of a 3D-printed elliptical resonator to probe acoustic vibration energy via a slit. The symbols of the main geometrical parameters of the elliptical resonator are shown in Figs. 2(b)–2(d).  $L$  and  $w$  represent the length of the elliptical resonator and the width of the slit, respectively, and  $2a$  and  $2b$  represent the major and minor axis lengths of the resonator cross section, respectively. The acoustic resonator was made of stainless-steel elliptical tube. The slit width  $w$  was set to 0.4 mm due to the restrictions of our processing technology, although a slimmer slit is beneficial to excite the one-dimensional longitudinal mode in the elliptical resonator.

The gap  $u$  between QTF and resonator was set as small as possible,<sup>13</sup> which is generally  $\sim 50 \mu\text{m}$ . The distance from the QTF tips to the resonator's axis was set to 0.7 mm.

In the off-beam configurations, detailed studies<sup>24</sup> showed that the optimum length of a resonator is between  $\lambda/2$  and  $\lambda$ , where  $\lambda$  is the sound wavelength. With the resonant frequency  $f$  of 32.7 kHz and the sound speed of 347 m/s, the sound wavelength is 1.14 cm. According to Fig. 1(b), the length and width of the spot at the entry and exit points of the  $\lambda$ -long resonator are 730 and 480  $\mu\text{m}$ , respectively. In order to allow the laser beam to clearly pass through all tested elliptical resonators, the elliptical tube of  $2a = 0.9$  mm and  $2b = 0.6$  mm was used with the beam waist located in the middle of the elliptical resonator.

The sound pressure distribution inside the ADM was subsequently simulated using COMSOL Multiphysics software based on finite element analysis (FEM) method, in order to determine the optimum resonator length. In our 3D model, the pressure acoustics module and the structural mechanics module were implemented. A spherical air domain was established, and its shell was set as a spherical perfectly matched layer (PML) to avoid the reflection of sound waves at the boundary. The laser power absorption was modeled as a line source through the center of the elliptical resonator. The eigenfrequency of the simulated QTF was 34.6 kHz. The sound source was mechanically coupled to the resonator and the QTF using fluid load boundary conditions. With the parameters of  $2a$ ,  $2b$ ,  $w$ ,  $u$ , and  $f$  fixed, Fig. 3(a) depicts the sound pressure distribution inside the ADM when  $L = 8.5$  cm. Figure 3(b) plots the values of the sound pressure along the center axis of the elliptical resonator for the different resonator lengths ( $L = 5.5, 6.5, 7.5, 8.5, 9.5, 10.5$  mm). When  $L = 5.5$  mm close to the half-wavelength of the sound waves, the simplest standing wave forms, whose only antinode is located in the middle of the elliptical resonator. However, its values of the sound pressure are the lowest in all resonators since the slit causes the leakage of the energy. When  $L = 10.5$  mm close to a wavelength, the standing wave with two antinodes forms. A M-shape sound pressure distribution is observed. Compared with  $L = 5.5$  mm, the higher values of the sound pressure can be obtained, as the node of the sound pressure is located in middle

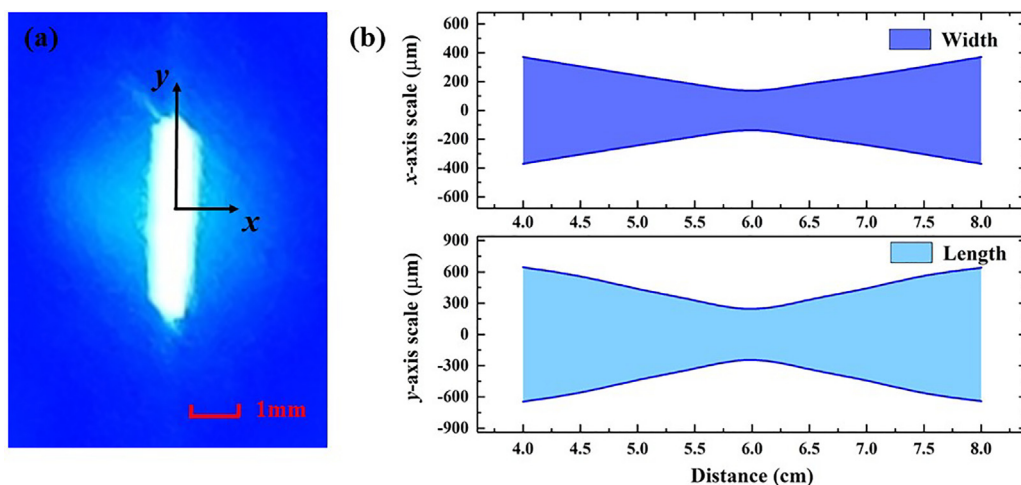


FIG. 1. (a) Snapshot of the used MLD emission profile. (b) Laser spot sizes at different distances from the lens.

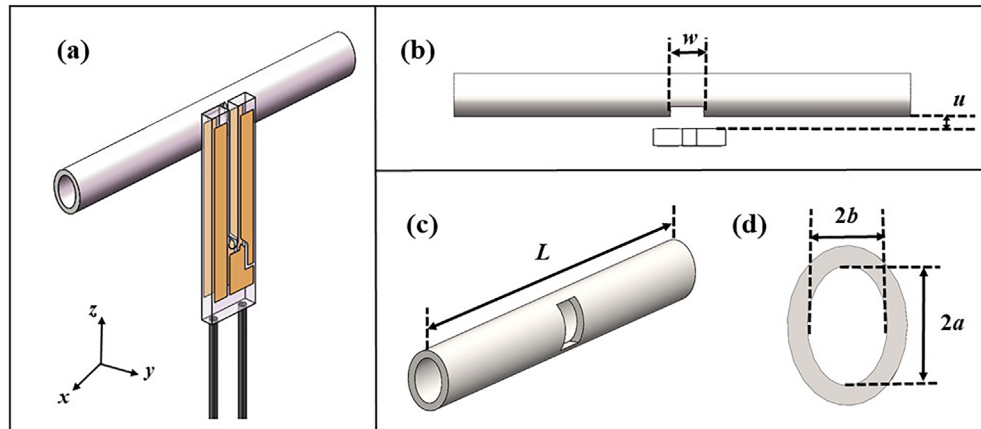


FIG. 2. (a) Schematic diagram of an ADM in EO-QEPAS. (b)–(d) Symbols of the geometric parameters of the elliptical resonator.

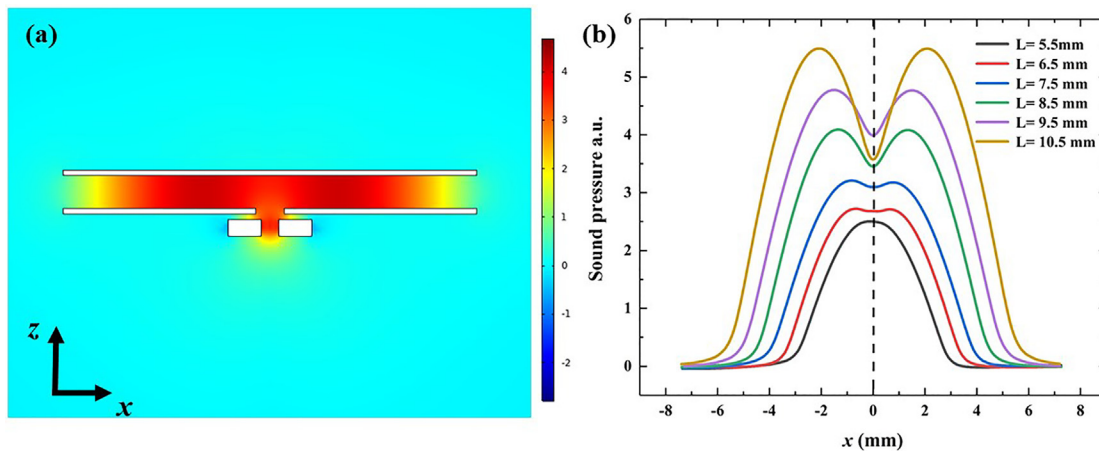


FIG. 3. (a) Sound pressure distribution of the ADM ( $L = 8.5$  cm) simulated by COMSOL Multiphysics software. (b) Simulated sound pressures along the center axis of the resonator for the different resonator lengths.

of the resonator and the slit does not act as an energy relief hole. The curves for  $L = 6.5, 7.5, 8.5,$  and  $9.5$  mm are the transition zone between half and a wavelength of the sound waves. According to Fig. 3(b), the maximum sound pressure in the middle of the resonator can be reached when  $L = 9.5$  mm.

The experimental setup is depicted in Fig. 4 to optimize the parameters of the elliptical resonator and assess the performance of the EO-QEPAS system. A commercial laser driver board (Wavelength Electronic Device, Model LDTC2/2) was used to generate 1 A injection current for the MLD. A function generator generated a square wave  $f = 32.7$  kHz, corresponding to the resonant frequency of the QTF, to modulate the amplitude of the laser current. The laser beam from the MLD was focused by a lens with 60 mm focal length, and an ADM was placed at the focal point. The photoacoustic signal output by the ADM was amplified by a low-noise transimpedance amplifier with a 10 M $\Omega$  feedback resistance and then directed to a lock-in amplifier

(Stanford Research Systems, Model SR830) for  $1f$  demodulation processing. The time constant of the lock-in amplifier was set to 300 ms combined with a 12 dB/oct filter slope corresponding to a detection bandwidth  $\Delta f$  of 0.833 Hz. The measurements were carried out at atmospheric pressure and room temperature. The needle valve was used to adjust the gas flow rate to a constant flow rate of 130 sccm to avoid the flow noise.

The elliptical resonator tubes of different lengths were prepared to experimentally compare their SNRs. The SNRs were calculated according to the following equation:  $SNR = (S_{QEPAS} - S_{BN})/1\sigma$ , where  $S_{QEPAS}$ ,  $S_{BN}$ , and  $1\sigma$  are the QEPAS signal amplitude, the background noise and the standard deviation of the noise, respectively. A sharp blade was used to make slits in the middle of these resonators. The lengths of the major and minor axes of all resonator tubes were 0.9 and 0.6 mm, respectively, and the slit widths were set to 0.4 mm. The MLD has an average output power of 176 mW after modulated



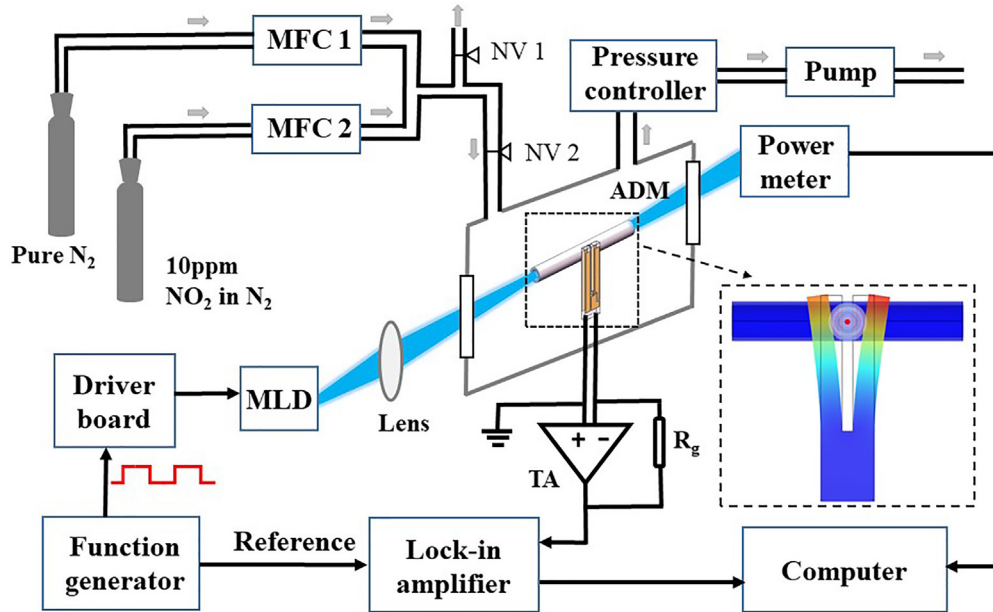


FIG. 4. Schematic diagram of the EO-QEPAS system.

by a 50% duty cycle square wave. The experimental results are shown in Fig. 5. The blue solid line plus circle symbols indicates the SNRs obtained by eight resonator tubes of different lengths at atmospheric pressure and room temperature when detecting a dry gas mixture with 1 ppm  $\text{NO}_2$  in  $\text{N}_2$ . With the resonator length increasing, the corresponding EO-QEPAS SNR increases, and when  $L = 9.5$  mm, the SNR reached the maximum value, which means that the strongest acoustic coupling between the QTF and the resonator was obtained. The simulated EO-QEPAS SNRs for nine resonators of different lengths was shown as the red solid line plus circle symbols. This simulated and

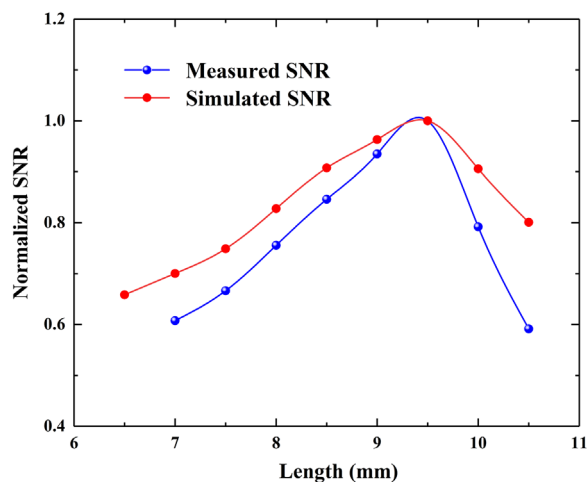


FIG. 5. Measured SNRs (blue circles) and simulated SNRs (red circles) as a function of the resonator length. The blue and red lines are the guide lines.

experimental results were in good agreement, which verifies the validity of our COMSOL model.

To assess the performance of EO-QEPAS, the measurement results obtained employing a bare QTF, a circular-tube off-beam QEPAS system (CO-QEPAS) and the EO-QEPAS system are summarized in Table I. The CO-QEPAS system has the optimum configuration of the circular resonator.<sup>24</sup> The signal and noise level were obtained by flushing the certified 1-ppm  $\text{NO}_2$ : $\text{N}_2$  gas mixture and pure  $\text{N}_2$  into the ADM. Based on Table I, the bare QTF has a large background noise due to the prong gap limit of the QTF. The background noise in the EO-QEPAS system is significantly reduced due to the optimal matching between the elliptical resonator and the beam profile. The EO-QEPAS system has a SNR gain factor of  $\sim 19$  compared to the bare QTF, while the CO-QEPAS system only has a SNR gain factor of  $\sim 6$ . With a 400 ppb  $\text{NO}_2$ : $\text{N}_2$  gas mixture, a SNR of 28 and a  $1\sigma$  detection limit of 14 ppb were obtained, corresponding to a normalized noise equivalent absorption (NNEA) of  $3.4 \times 10^{-8} \text{ cm}^{-1} \text{ W/Hz}^{1/2}$ .

In conclusion, the EO-QEPAS technique was demonstrated to efficiently operate with an MLD as the excitation light source in QEPAS. It is well known that the value of SNR is determined by signal amplitude together with noise level. Although the signal amplitude can be significantly enhanced through the increase in the optical power in QEPAS, the growing part of the signal amplitude is usually balanced out by the noise that grows more due to the mismatch between the resonator and beam shape. The elliptical resonator is proposed specifically for a strip-shaped laser beam, which allows us to fully utilize the optical power with a low noise output. Further topics of interest include building the theoretical model of the elliptical resonator and finding the analytical solutions of acoustic modes, as well as developing the trace gas sensors based on EO-QEPAS.

**TABLE I.** Intercomparison of a bare QTF, a CO-QEPAS and EO-QEPAS systems. ID: inner diameter of circular resonator;  $1\sigma$ : the standard deviation of the noise.

	Resonator geometric parameters (mm)				Signal (mV)	Background (mV)	$1\sigma$ ( $\mu$ V)	SNR
	ID	$2a$	$2b$	L				
CO-QEPAS	0.8	...	...	9.5	1.41	0.93	2.8	169
EO-QEPAS	...	0.9	0.6	9.5	1.65	0.33	2.3	575
Bare QTF					18.73	18.49	8.0	30

The project was sponsored by the National Key R&D Program of China (No. 2019YFE0118200), National Natural Science Foundation of China (Nos. 62175137, 62122045, and 62075119), Shanxi Science Fund for Distinguished Young Scholars (No. 20210302121003), Sanjin Scholar (No. 2017QNSJXZ-04), and Shanxi “1331KSC.”

## AUTHOR DECLARATIONS

### Conflict of Interest

The authors have no conflicts to disclose.

### Author Contributions

Z.S. and H.W. contributed equally to this work.

### DATA AVAILABILITY

The data that support the findings of this study are available from the corresponding author upon reasonable request.

## REFERENCES

- N. Petra, J. Zweck, A. A. Kosterev, S. E. Minkoff, and D. Thomazy, *Appl. Phys. B* **94**, 673 (2009).
- A. A. Kosterev, L. Dong, D. Thomazy, F. K. Tittel, and S. Overby, *Appl. Phys. B* **101**, 649 (2010).
- X. Yin, L. Dong, H. Zheng, X. Liu, H. Wu, Y. Yang, W. Ma, L. Zhang, W. Yin, L. Xiao, and S. Jia, *Sensors* **16**, 162 (2016).
- Y. Ma, Y. He, L. Zhang, X. Yu, J. Zhang, R. Sun, and F. K. Tittel, *Appl. Phys. Lett.* **110**, 031107 (2017).
- Z. Wang, Q. Wang, J. Y. Ching, J. C. Wu, G. Zhang, and W. Ren, *Sens. Actuators, B* **246**, 710 (2017).
- K. Hong and J. Kim, *J. Sound Vib.* **183**, 327 (1995).
- A. A. Kosterev, Y. A. Bakhrin, R. F. Curl, and F. K. Tittel, *Opt. Lett.* **27**, 1902 (2002).
- P. Patimisco, G. Scamarcio, F. K. Tittel, and V. Spagnolo, *Sensors* **14**, 6165 (2014).
- H. Yi, R. Maamary, X. Gao, M. W. Sigrist, E. Fertein, and W. Chen, *Appl. Phys. Lett.* **106**, 101109 (2015).
- V. Spagnolo, A. A. Kosterev, L. Dong, R. Lewicki, and F. K. Tittel, *Appl. Phys. B* **100**, 125 (2010).
- Z. Shang, S. Li, H. Wu, and L. Dong, *Appl. Sci.* **10**, 1197 (2020).
- H. Wu, L. Dong, H. Zheng, Y. Yu, W. Ma, L. Zhang, W. Yin, L. Xiao, S. Jia, and F. K. Tittel, *Nat. Commun.* **8**, 15331 (2017).
- L. Dong, A. A. Kosterev, D. Thomazy, and F. K. Tittel, *Appl. Phys. B* **100**, 627 (2010).
- M. Jahjah, W. Jiang, N. P. Sanchez, W. Ren, P. Patimisco, V. Spagnolo, S. C. Herndon, R. J. Griffin, and F. K. Tittel, *Opt. Lett.* **39**, 957 (2014).
- S. Li, L. Dong, H. Wu, A. Sampaolo, P. Patimisco, V. Spagnolo, and F. K. Tittel, *Anal. Chem.* **91**, 5834 (2019).
- S. Borri, P. Patimisco, A. Sampaolo, H. E. Beere, D. A. Ritchie, M. S. Vitiello, G. Scamarcio, and V. Spagnolo, *Appl. Phys. Lett.* **103**, 021105 (2013).
- T. Wei, A. Zifarelli, S. Dello Russo, H. Wu, G. Menduni, P. Patimisco, A. Sampaolo, V. Spagnolo, and L. Dong, *Appl. Phys. Rev.* **8**, 04149 (2021).
- H. Zheng, L. Dong, X. Yin, X. Liu, H. Wu, L. Zhang, W. Ma, W. Yin, and S. Jia, *Sens. Actuators, B* **208**, 173 (2015).
- H. Zheng, L. Dong, Y. Ma, H. Wu, X. Liu, X. Yin, L. Zhang, W. Ma, W. Yin, L. Xiao, and S. Jia, *Opt. Express* **24**, A752 (2016).
- P. Patimisco, A. Sampaolo, M. Giglio, S. Russo, V. Mackowiak, H. Rossmadl, A. Cable, F. K. Tittel, and V. Spagnolo, *Opt. Express* **27**, 1401 (2019).
- P. Patimisco, A. Sampaolo, M. Giglio, V. Mackowiak, H. Rossmadl, B. Gross, A. Cable, F. K. Tittel, and V. Spagnolo, *Opt. Lett.* **43**, 1854 (2018).
- H. Wu, X. Yin, L. Dong, K. Pei, A. Sampaolo, P. Patimisco, H. Zheng, W. Ma, L. Zhang, W. Yin, L. Xiao, V. Spagnolo, S. Jia, and F. K. Tittel, *Appl. Phys. Lett.* **110**, 121104 (2017).
- Q. Wang, Z. Wang, W. Ren, P. Patimisco, A. Sampaolo, and V. Spagnolo, *Sens. Actuators, B* **268**, 512 (2018).
- K. Liu, X. Guo, H. Yi, W. Chen, W. Zhang, and X. Gao, *Opt. Lett.* **34**, 1594 (2009).
- H. Yi, W. Chen, S. Sun, K. Liu, T. Tan, and X. Gao, *Opt. Express* **20**, 9187 (2012).
- Y. Ma, Y. Hong, S. Qiao, Z. Lang, and X. Liu, *Opt. Lett.* **47**, 601 (2022).
- M. Lassen, L. Lamard, Y. Feng, A. Peremans, and J. C. Petersen, *Opt. Lett.* **41**, 4118 (2016).
- R. Rousseau, Z. Lohmari, M. Bahriz, K. Chamassi, R. Teissier, A. N. Baranov, and A. Vicet, *Opt. Express* **27**, 7435 (2019).